Article

Kinetic pathways of gyroid-to-cylinder transitions in diblock copolymers under external fields: cell dynamics simulation

Pinna, Marco and Zvelindovsky, Andrei V.

Pinna, Marco and Zvelindovsky, Andrei V. (2008) Kinetic pathways of gyroid-to-cylinder transitions in diblock copolymers under external fields: cell dynamics simulation. Soft Matter, 4 (2). pp. 316-327. ISSN 1744-683X

It is advisable to refer to the publisher's version if you intend to cite from the work.
http://dx.doi.org/10.1039/B706815H

Kinetic pathways of gyroid-to-cylinder transitions in diblock copolymers under external fields: cell dynamics simulation

Marco Pinna and Andrei V. Zvelindovsky*

Received 10th May 2007, Accepted 30th October 2007
First published as an Advance Article on the web 21st November 2007
DOI: 10.1039/b706815h

Using cell dynamics simulation we investigate the cubic gyroid morphology of block copolymer melts under simple shear flow and electric field. The electric field should be stronger than a certain critical value to induce transition to a cylindrical phase. In the case of simple steady shear the gyroid-to-cylinder transition was observed even for a very weak shear. Quantitative analysis of pathways of gyroid-to-cylinder transition is performed by means of Minkowski functionals. We found that the kinetics of the gyroid-to-cylinder transition are different under electric field and shear flow. Moreover, the gyroid structure under different strengths of electric field shows different pathways. Different types of intermediates such as five-, four-fold connections and "winding" cylinders are found for different pathways.

I. Introduction

Block polymers are chain molecules which are composed of chemical different blocks covalently connected into one macromolecule. They belong to an important class of materials that, due to their nature, can self-assemble into different nanostructures.[1] These can be lamellae, hexagonally packed cylinders (C), body centred cubic and complex structures like the gyroid structure (G). There is a vast number of experimental and theoretical works which address the problem of tailoring a desired nanostructure.[2] Applied external fields are promising candidates to achieve that goal. Such fields can be surface fields,[3,4] electric fields[5,6] and shear flow.[7] Until now only the behaviour of classical structures (lamellae, cylinders and spheres) under external fields received a comprehensive experimental and theoretical treatment.[1,5,6,8] The fundamental understanding of complex structures like the gyroid structure is still limited. A nice theoretical description of the gyroid phase can be found in a work by Schick with the self-explaining title "Avatars of the gyroid".[9] The gyroid is a continuous cubic structure with $Ia\bar{3}d$ symmetry, in which the minority domains form interweaving left- and right-handed three-fold coordinated lattices.[10] Taking advantage of its complex domain structure, the gyroid is expected to have a large applicability, for instance, as three-dimensional photonic crystals, microporous systems, nanoreactors, *etc.*[1,11–14] The first step on the way towards an application is to understand how a given structure behaves under external fields, what phase transitions can be induced by these fields, and how these transitions evolve over time. Recently, several experiments have been performed on the stability of the gyroid structure and corresponding phase transitions.[15–17] Using simultaneous small angle scattering and rheology Vigild *et al.*[15] examined the macroscopic dynamical response and the mesoscopic structural behaviour. Eskimergen *et al.*[16] studied the stability of the gyroid phase using combined oscillated shear and small angle neutron scattering techniques. They showed that the gyroid phase of a polystyrene–polyisoprene diblock copolymer is unstable when exposed to large amplitude high-frequency shear deformation. Imai *et al.*[17] investigated the kinetic pathway of a lamellar-to-gyroid transition by means of small angle X-ray scattering.

Several theoretical techniques were used as well.[10,18–20] Honda and Kawakatsu studied the transition from the G structure into a hexagonally packed cylinder induced by an external shear flow by means of self-consistent field theory.[18] Giupponi and co-workers applied lattice Boltzmann technique to study the rheological properties of gyroid structures.[21,22] Nonomura *et al.*[19] studied the transition of the G structure into lamellar and hexagonal C structure by means of the amplitude equations. Matsen studied gyroid-to-cylinder transitions under temperature change with self-consistent field theory.[23] Very recently we studied electric field-induced gyroid-to-cylinder transitions using self-consistent field theory.[24]

There is no analytical approach to treat the gyroid phase under shear flow. The only two sheared phases which have been fully studied by analytical theory are lamellae and cylinders.[25,26]

No experimental results on the gyroid phase under an electric field have been reported in the literature.

The purpose of the present paper is to study the kinetic pathways of the gyroid-to-cylinder phase transition under external fields using cell dynamics simulation (CDS). We unravel various intermediate structures involved in the transition.

Cell dynamics simulation is based on simpler Hamiltonians than those used in self-consistent field theory (SCFT). Comparing our findings with ones of self-consistent field theory[18,24] can allow determination of whether the reduced Hamiltonian description can produce the same kinetic pathways as the full self-consistent field treatment. Being much faster, CDS can serve as a research precursor for a SCFT study

Centre for Materials Science, Department of Physics, Astronomy and Mathematics, University of Central Lancashire, Preston, United Kingdom PR1 2HE. E-mail: avzvelindovsky@uclan.ac.uk

of complex phases. In addition, it can serve as a fast link with experimental studies. Modern experiments can resolve intermediate structures in phase transitions using transmission electron microscopy (TEM). An example of a non trivial intermediate in the sphere-to-cylinder transition is given in ref. 5 Therefore, a real-space computer simulation of such intermediates becomes increasingly important. We found a wider range of intermediate structures in the transition under an electric field compared to our earlier SCF study.[24] We hope that the present paper will stimulate new experiments on the gyroid phase under an electric field to verify these findings. The Appendix gives details of the Minkowski functionals calculation.

The paper is organised as follows. In Section II we present the cell dynamics simulation algorithm. In Section III we discuss the results obtained under external fields, before drawing conclusions in Section IV.

II. The cell dynamics simulation

The cell dynamics simulation method is well established in the literature[27–33] and it is a very promising model to describe morphologies and the behaviour of diblock copolymers. In the cell dynamics simulation an order parameter $\psi(t, i)$ is determined at time t in the cell i of a discrete lattice. For an AB diblock copolymer we use the difference between the local and global volume fractions:

$$\psi = \phi_A - \phi_B + (1 - 2f) \tag{1}$$

where ϕ_A and ϕ_B are the local volume fractions of A and B monomers respectively, and f is the volume fraction of A monomers in the diblock, $f = N_A/(N_A + N_B)$.

The time evolution of the order parameter under a macroscopic flow is given by a Cahn–Hilliard–Cook (CHC) equation:[27,28]

$$\frac{\partial\psi}{\partial t} + \nabla\cdot(v\psi) = M\nabla^2\left(\frac{\delta F[\psi]}{\delta\psi}\right) + \eta\xi(\boldsymbol{r},t) \tag{2}$$

where $\boldsymbol{v} = (v_x, v_y, v_z)$ is the flow, M is a phenomenological mobility constant. Here we set $M = 1$ which correspondingly sets the timescale for the diffusive processes (the dimensionless time is tM/a_0^2, where the lattice cell size a_0 is set to 1). The last term in eqn (2) is a noise with amplitude η and $\xi(\boldsymbol{r},t)$ being a Gaussian random noise.[34,35] The free energy functional (divided by kT) is:[29]

$$\begin{aligned} F[\psi(\boldsymbol{r})] = &\int d\boldsymbol{r}\left[H(\psi) + \frac{D}{2}|\nabla\psi|^2\right] \\ &+ \frac{B}{2}\int d\boldsymbol{r}\int d\boldsymbol{r}' G(\boldsymbol{r}-\boldsymbol{r}')\psi(\boldsymbol{r})\psi(\boldsymbol{r}') \end{aligned} \tag{3}$$

where

$$H(\psi) = \left[-\frac{\tau}{2} + \frac{A}{2}(1-2f)^2\right]\psi^2 + \frac{v}{3}(1-2f)\psi^3 + \frac{u}{4}\psi^4 \tag{4}$$

with τ being a temperature-like parameter and A, v, u, D being phenomenological constants.[30,31] The Laplace equation Green function $G(\mathbf{r} - \mathbf{r}')$ satisfies $\nabla^2 G(\mathbf{r} - \mathbf{r}') = -\delta(\mathbf{r} - \mathbf{r}')$, and B is a parameter that introduces a chain-length dependence to the free energy.[31] We consider a steady shear defined by:

$$v_z = \dot{\gamma}y,\ v_x = v_y = 0 \tag{5}$$

where we take the z-axis in the flow direction, y-axis in the velocity gradient direction and the x-axis is the vorticity axis. The dimensionless shear rate is $\tilde{\dot{\gamma}} = \dot{\gamma}a_0^2/M$ and we use the dimensionless coordinate $\tilde{y} = y/a_0$. When a shear flow is applied in the z-direction, the following shifted periodic boundary condition must be used:[34]

$$\psi(x, y, z, t) = \psi(x + N_xL, y + N_yL, z + N_zL + \gamma(t)N_yL, t) \tag{6}$$

where N_x, N_y, N_z are arbitrary integers and L is the box size.

When an electric field along the x-axis is applied and no flow is present, the evolution equation for a diblock copolymer melt is:[36,37]

$$\frac{\partial\psi}{\partial t} = \tilde{\alpha}\nabla_x^2\psi + \nabla^2\left(\frac{\delta F[\psi]}{\delta\psi}\right) + \eta\xi(\boldsymbol{r},t) \tag{7}$$

where

$$\tilde{\alpha} = \frac{\varepsilon_0(\varepsilon_A - \varepsilon_B)^2}{\varepsilon_A f + \varepsilon_B(1-f)}\frac{E_0^2 v}{kT} \tag{8}$$

Here ε_0 is the vacuum permittivity, v is the volume of one polymer chain, ε_A and ε_B are the dielectric constants of the A and B blocks respectively, and E_0 is the strength of the electric field.[38] Ref. 37 contains extensive discussion of the electric field estimated for real experimental systems [*e.g.* the electric field 8 V μm^{-1} corresponds to $\tilde{\alpha}$ = 0.1 for a typical experimental system of a polystyrene–polymethyl methacrylate (PS–PMMA) diblock copolymer]. In the presence of an electric field and a steady shear the CDS equation becomes:

$$\begin{aligned} \psi(\boldsymbol{n}, t+1) = &\psi(\boldsymbol{n}, t) - \{\langle\langle\Gamma(\boldsymbol{n}, t)\rangle\rangle - \Gamma(\boldsymbol{n}, t) \\ &+ B\psi(\boldsymbol{n}, t) - \eta\xi(\boldsymbol{n}, t) \\ &+ \frac{1}{2}\tilde{\dot{\gamma}}\tilde{y}\left[\psi(n_x, n_y, n_z+1, t)\right. \\ &\left.-\psi(n_x, n_y, n_z-1, t)\right] \\ &-\tilde{\alpha}\left[\psi(n_x+1, n_y, n_z, t)\right. \\ &+\psi(n_x-1, n_y, n_z, t) \\ &\left.-2\psi(n_x, n_y, n_z, t)\right]\} \end{aligned} \tag{9}$$

For simple diffusion dynamics, eqn 2 is found to be very appropriate to describe phase transitions in block copolymer morphologies. In our recent work we showed that such dynamics (with a different free energy model) quantitatively describe experimental kinetics of cylinder-to-perforated lamellae transition in thin films.[39]

III. Results

We study the behaviour of the gyroid phase under applied electric field and simple steady shear. All simulations were performed using (shifted) periodic boundary conditions, eqn 6.

A. Initial gyroid structure

In our previous paper we obtained a phase diagram for a diblock copolymer melt by means of CDS (Fig. 1 in ref. 33) in agreement with earlier work.[31] The subject of our interest is the gyroid phase. We expect the gyroid structure to be present in the region of the phase diagram where we observe a bicontinuous structure. We note that the term "bicontinuous" cannot be understood uniquely. The gyroid is more correctly named a double gyroid (indeed, an often used term), where each of the block components forms two non-intersecting continuous networks. In the case of a defected structure, where these networks have necks between them, there are still two continuous networks — one for each block component of the diblock copolymer. In the case of lamellae, spheres or cylinders, there is at most one component which is continuous. Due to an inherent feature of the gyroid structure, the tree-arm connections, a spontaneously formed structure has many defects, as seen in Fig. 1a. To obtain a perfect gyroid starting from a homogeneous melt CDS would take time beyond any reasonable limit. As the purpose of our paper is different, we employ the method of gyroid generation proposed in ref. 18. We start from a regular structure:[18]

$$\psi(x, y, z) = \left\{ \cos\frac{2\pi x}{D_G}\sin\frac{2\pi y}{D_G} + \cos\frac{2\pi y}{D_G}\sin\frac{2\pi z}{D_G} + \cos\frac{2\pi z}{D_G}\sin\frac{2\pi x}{D_G} \right\}^2 - 1 \quad (10)$$

where x, y and z are Cartesian coordinates. The use of the squared form on the right-hand side of eqn (10) originates from the fact that the gyroid structure is formed by two networks, each with the G symmetry.[18] From eqn (1) it follows that our order parameter can be as positive as negative. Because of that we add -1 to the right-hand side of eqn (10) to ensure the proper work of the CDS code. To calculate the side length of the unit cell of the G structure, D_G, we use the following procedure. Fig. 1b shows the result of the transition of the bicontinuous structure from Fig. 1a to cylinders under an applied electric field. We use this result to calculate the average distance between cylinders (D_C) that appears to be *ca.* 7–7.5 grid points (the whole simulation box is 128 × 128 × 128 grid points). Assuming epitaxial G-to-C transition and using $D_G = \sqrt{6}D_C$[eqn (14) from ref. 18] we obtain $D_G \approx 17$–18 grid points. We choose $D_G = 17.2$ which is the same as in ref. 18. To demonstrate that our final cylindrical structure (Fig. 1b) is not a stable phase, we switched off the electric field and continued the simulation with the noise added. Fig. 1c, d, e illustrate the results for different time steps. For the sake of simplicity we show only a crop of the simulation box. Initially perfect cylinders (Fig. 1c) develop undulations (Fig. 1d) which grow in time (Fig. 1e). Eqn (10) generates a regular gyroid structure as shown in Fig. 2a (left) in a box of 64 × 64 × 64 grid points. Fig. 2a (right) shows the view of the structure along the [111] direction. The structure remains stable after 1 000 000 time steps of equilibration[33] (see Fig. 2b). The equilibrated gyroid, Fig. 2b, is only slightly different from the initial structure, Fig. 2a. The change in thickness of the networks is due to the equilibration process and has no effect on the symmetry. Along the border of the simulation box there is a slight difference between these structures: the connections in snapshot (b) have somewhat different orientation compared to the initial ones in (a). This is likely to be a result of a slight mismatch of the simulation box size with the G unit cell size D_G. Due to the sufficiently large simulation box this has no noticeable effect on the reported results.

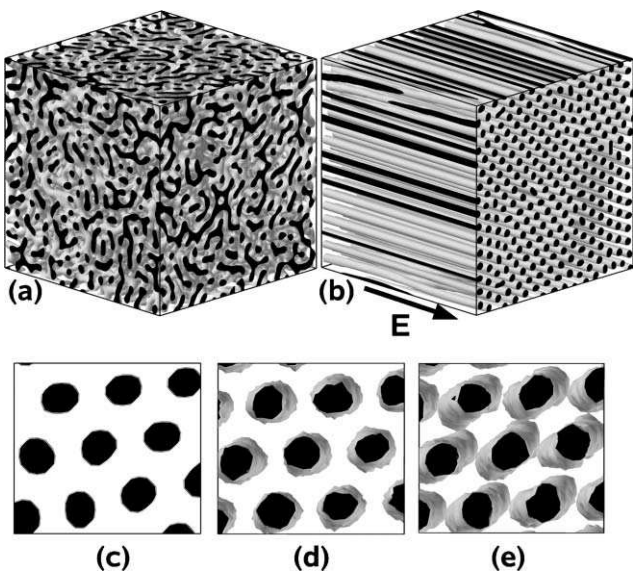

Fig. 1 (a) Bicontinuous structure after 200 000 time steps. The parameters used in eqn (3,4) are $A = 1.5$; $B = 0.02$; $D = 0.5$; $v = 2.3$; $u = 0.38$; $f = 0.45$; $\tau = 0.33$. (b) The structure after 500 000 time steps under an electric field ($\tilde{\alpha}$=0.1) applied to the structure (a). The field direction is indicated by $\vec{E}$. (c) Crop of image (b) viewed from the electric field direction. (d) The structure after 85 000 time steps without an electric field [starting from structure (c)] with the noise. (e) The structure after 500 000 time steps without electric field with the same noise.

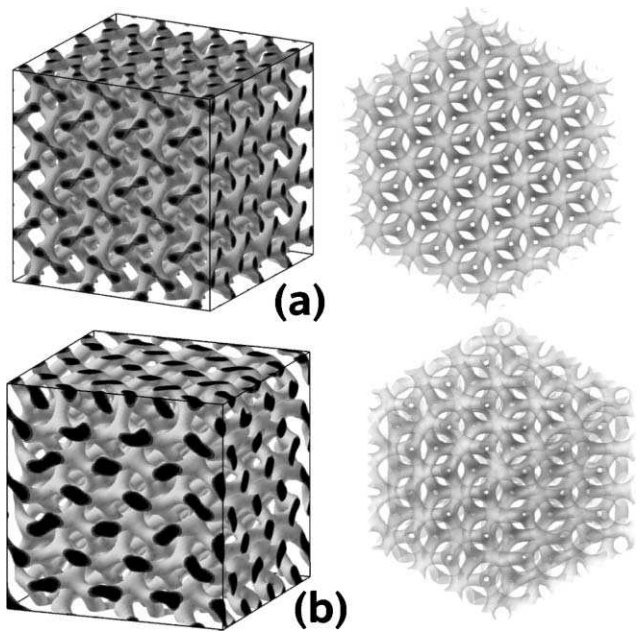

Fig. 2 The gyroid structure (3D view, left, and the view along [111] direction, right): (a) Initial structure; (b) the structure after 1 000 000 time steps of equilibration.

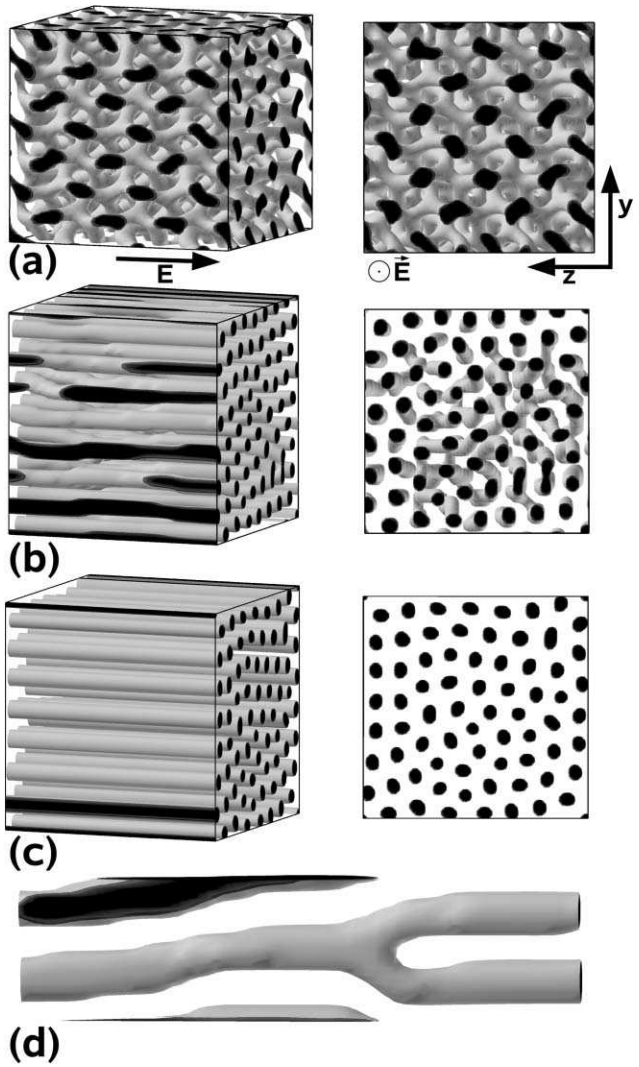

Fig. 3 The gyroid structure under different electric fields: $\tilde{\alpha}$ = (*a*) 0.001; (b) 0.01; (c) 0.1; all structures are after 100 000 time steps. Left: 3D view. Right: side view. (d) A characteristic defect from (b).

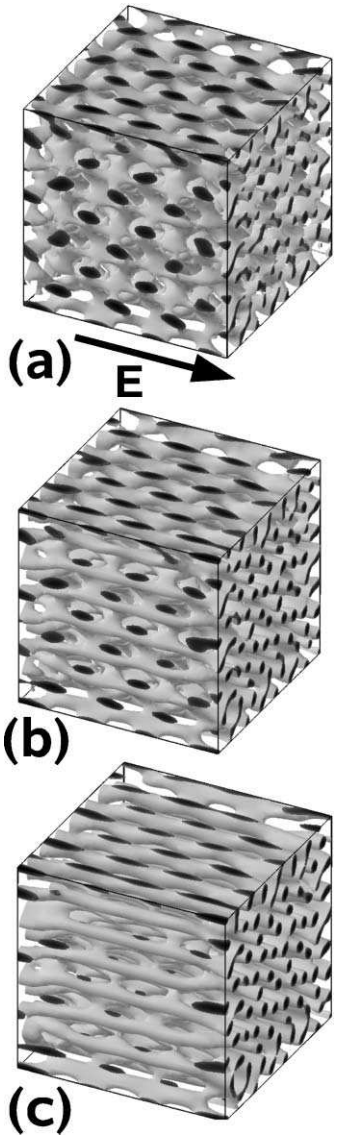

Fig. 4 Kinetics of the gyroid-to-cylinder transition under an electric field ($\tilde{\alpha} = 0.1$). *Timesteps* : (*a*)60; (*b*)100; (*c*)160.

B. The gyroid structure under an electric field

First, we report results on the effect of an applied electric field on the gyroid structure. In all simulations the electric field was applied along the *x*-direction.

When the electric field is very weak $\tilde{\alpha}$ = 0.001, we observe no structural change (see Fig. 3a). A similar situation was observed in the case of spheres under a weak electric field (*cf.* Fig. 2a in ref. 33). To induce the gyroid-to-cylinder transition an electric field with a strength above some critical value is required, Fig. 3b. Initially the cylinders have some imperfections: there are interconnections between neighbouring cylinders, often forming fork-like disclination as shown in Fig. 3d. If we continue the simulation run to 300 000 time steps these defects disappear. The stronger field over the shorter time is required to annihilate defects in cylinders. When a strong electric field is applied we observe the gyroid-to-cylinder transition with all cylinders parallel to the *x*-direction. All cylinders span the whole box (see Fig. 3c) but their hexagonal packing has many typical defects in the form of 5–7 pairs, Fig. 3c. Fig. 4 shows the kinetics of the transition for the system from Fig. 3c. In the first snapshot of Fig. 4a (after 60 time steps) we see the connections being extended and new connections are formed along the *x*-direction. In snapshot (b) we observe the formation of cylinder backbones along the electric field direction. There are many interconnections perpendicular to the electric field lines. They start to break as shown in snapshot (c).

In Fig. 5 we show the gyroid structure with the (100) plane perpendicular to the electric field direction. All images are thin slices from the middle of the simulation box. Initially, the structure is very regular (a). At the first stage, the G structure becomes thinner as a result of applying an electric field, Fig. 5b. The electric field does not melt the G structure completely. As is shown in snapshot (c), the electric field makes the connections, which are perpendicular to the electric field, thinner and induces further connections, which are parallel to the electric field lines. These connections are formed in an epitaxial way growing from the parent G structure. The

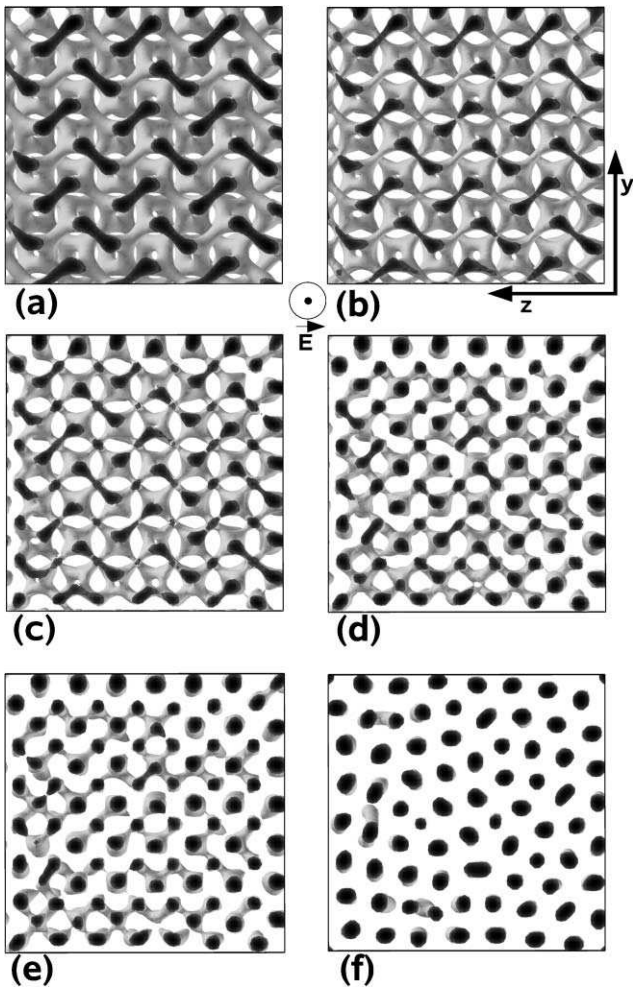

Fig. 5 Kinetics of the gyroid-to-cylinder transition from Fig. 4 ($\tilde{\alpha}$ = 0.1) in the (100) plane view. Time steps: (a) 10; (b) 40; (c) 100; (d) 160; (e) 200; (f) 3000.

snapshots (d–e) illustrate the breaking of the perpendicular connections and enhancement of the parallel cylinders (seen as black spots). We observe that the cylinders are not uniform in their diameters. Breakage of the interconnections occurs non-uniformly as well, Fig. 5e, leading to defects in the hexagonal packing of the cylinders as is shown in snapshot (f).

C. The gyroid structure under shear flow

In this subsection we describe the behaviour of the gyroid structure under simple steady shear flow. First, we consider the gyroid system under a weak shear. We take the z-axis in the flow direction, the y-axis being the velocity gradient and x being the vorticity axis. The final structure is shown in Fig. 6a. The total shear strain ($\gamma = \dot{\gamma}t$) during this simulation is $\gamma = 50$ (5000%). We obtain a cylindrical structure with many defects. Although the cylinders are aligned along the flow direction, they have many interconnections both in the shear plane and perpendicular to the shear plane. The ordering in the vorticity plane (x–y plane) is high with only a few defects in the hexagonal lattice. Fig. 6b shows the result for a higher shear rate. The total shear strain is the same as before, $\gamma = 50$, yet the result is very different. The cylinders are aligned along the

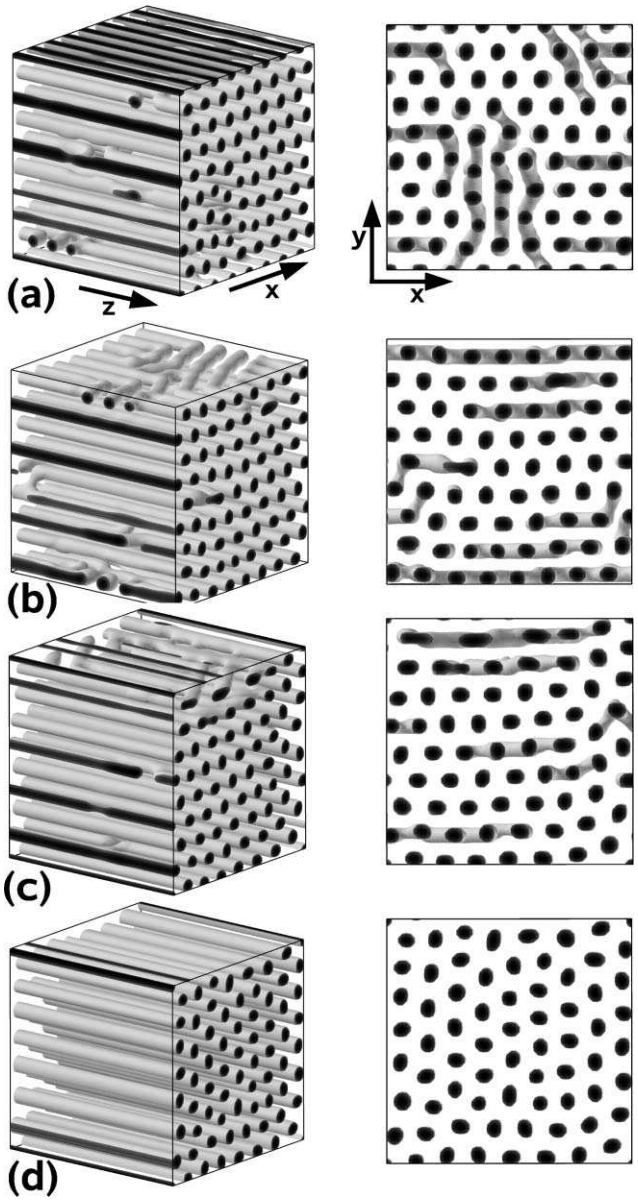

Fig. 6 Gyroid under different shear rates $\tilde{\dot{\gamma}}$: (a) 0.0001; (b) 0.0005; (c) 0.001; (d) 0.005. Left: 3D view. Right: vorticity plane view.

shear direction and most interconnections lie in shear plane. The shear is too weak to destroy the connections completely. However, it is sufficient to destroy almost all connections between different shear planes, confirming that cylinders in different shear planes slide with respect to each other. Increase of the shear rate results in fewer interconnections between cylinders compared to the case in Fig. 6a (see Fig. 6c). At very strong shear the cylinders have no interconnections but their hexagonal packing has many defects in the form of characteristic 5–7 pairs, Fig. 6d. Remarkably, the weaker the shear is the fewer defects are in the hexagonal packing (*cf.* Fig. 6a and d). Therefore, the kinetic pathway (for instance, the order, in which interconnections are annihilated) affects the final structure.

Fig. 7 shows the time evolution of the gyroid-to-cylinders transition for the system from Fig. 6c. At the early stage (γ = 0.5, Fig. 7a) the shear does not disturb the structure to a large

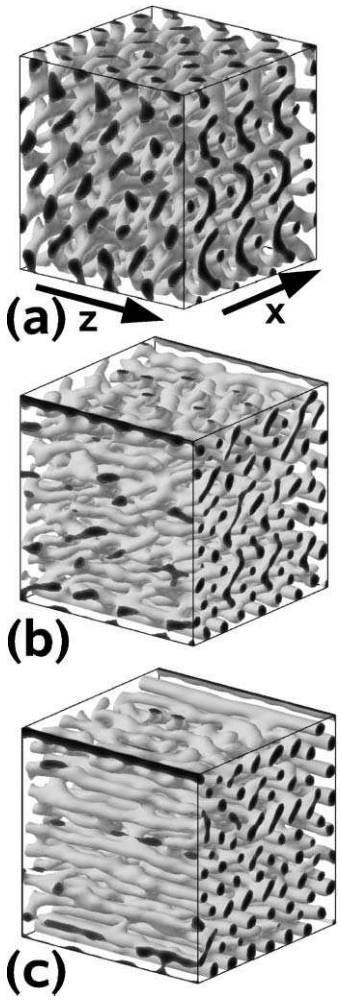

Fig. 7 Kinetics of the gyroid-to-cylinder transition under shear, $\dot{\gamma}$ = 0.005. Time steps: (a) t = 100 (γ = 0.5); (b) t = 700 (γ = 3.5); (c) t = 1000 (γ = 5).

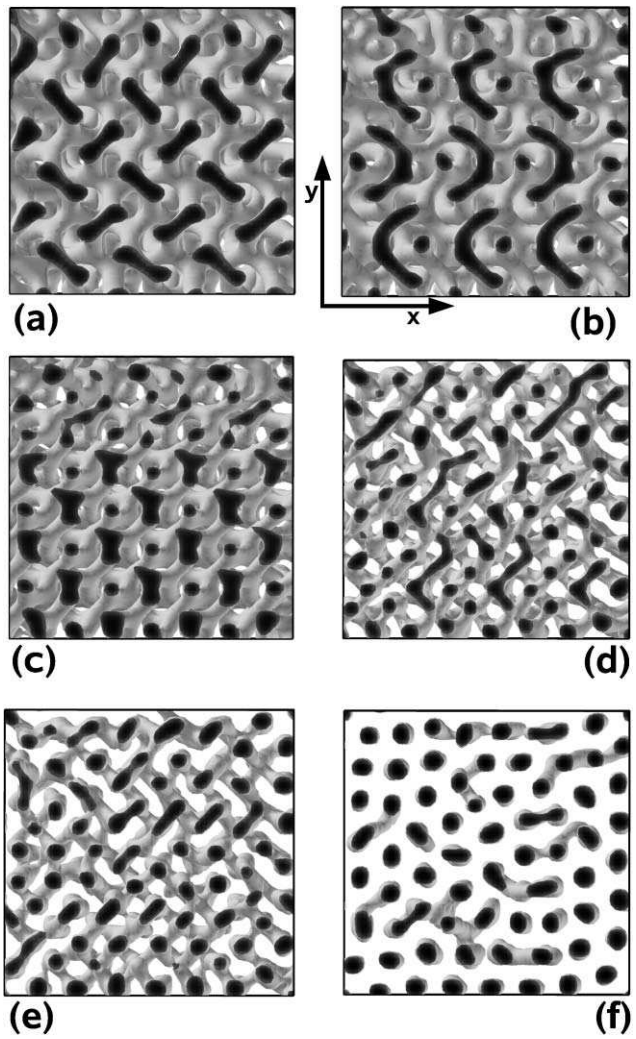

Fig. 8 Kinetics of the transition from Fig. 7 viewed in the (100) plane. Time steps: (a) 10 (γ = 0.05); (b) 100 (γ = 0.5); (c) 200 (γ = 1); (d) 700 (γ = 3.5); (e) 1000 (γ = 5); (f) 3000 (γ = 15).

extent. At γ = 3.5 (Fig. 7b) we observe the formation of the first little cylinders tilted with respect to the shear direction. A highly interconnected network, which is characteristic for the G phase, is still present but it is deformed. At γ = 5, Fig. 7c, the shear starts to break the connections which are perpendicular to the shear flow, and the first cylinders are formed which span the whole box. We show another view of the process in Fig. 8. Although, there is no noticeable change in the bulk of the G structure between the time steps of Fig. 8a and b, the side view shows a drastic change, Fig. 8a and b. This is due to the fact that the G structure flows without global change, and snapshots (a) and (b) are the cuts of the box at different points of the G structure. At a later time the structure becomes thinner, Fig. 8c. The last snapshots (d)–(f) show the formation of cylinders in the flow direction and breakage of the interconnections perpendicular to the flow.

D. Pathways of gyroid-to-cylinder transition under an electric field and shear flow

In this subsection we compare the gyroid-to-cylinder transition under an electric field and simple steady shear flow in more detail. The left column of Fig. 9 shows results for the system under an electric field. At 40 time steps we observe the formation of new connections along the field direction (a). There are five-fold connections (b) which we describe in more detail in the next subsection. The five-fold connections have been found as intermediates in the G-to-C transition under temperature change in ref. 23. In snapshot (c) we observe that connections, which are along the electric field, become thicker whilst the ones perpendicular to the field lines become thinner. In snapshot (d) the electric field breaks the connections which are perpendicular to the field direction, and the first cylinders are formed. In the last two snapshots we observe the final breakage of the connections and the formation of cylinders that span the whole box. When the gyroid structure is subjected to a steady shear flow the behaviour is different, Fig. 9 (right column). In the snapshots (a) and (b) we observe that the G structure flows without much change. After 160 time steps, snapshot (d), we observe the contraction of connections which are perpendicular to the direction of the vector $\overrightarrow{gradient} + \overrightarrow{shear}$ and the extension of connections which

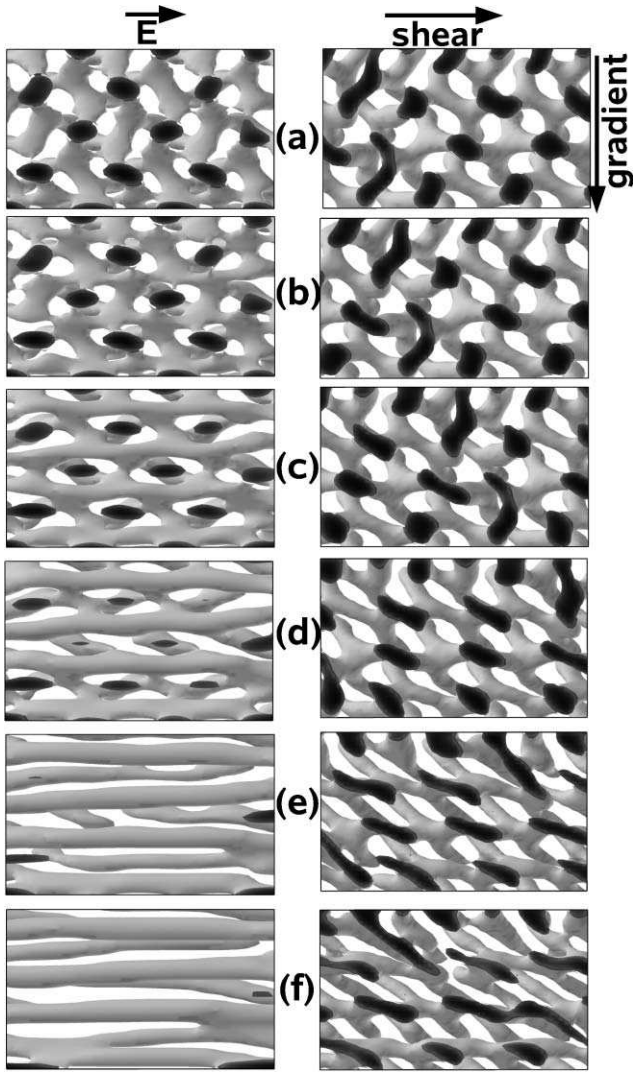

Fig. 9 Kinetics of gyroid-to-cylinder transition under an electric field ($\tilde{\alpha} = 0.1$ − left) and shear flow ($\dot{\gamma} = 0.005$ − right). Time steps: (a) 40; (b) 60; (c) 100; (d) 160; (e) 300; (f) 400. Directions of electric field, shear flow and velocity gradient are indicated by arrows.

are along this vector. It leads to the formation of four-fold connections [snapshots (d,e)]. In the last snapshot, (f), we observe that the connections start to break and the first cylinders form. These cylinders are tilted with respect to the shear direction. The tilt is determined by the gradient direction.

E. Comparative kinetics from Minkowski functionals

In the previous section we described pathways of the gyroid-to-cylinder transition under applied electric field and shear flow by describing real-space 3D images. Visual inspection of such images in cases of very complex interconnected structures is not an easy task. In modern theoretical physics the analysis of complex patterns is often done with the help of Minkowski functionals.[42] For a 3D structure/image there are four Minkowski functionals: volume (V), surface area (S), integral mean curvature ($2H$) and Euler characteristic (χ).[42–45] The Euler characteristic is directly related to the integral Gaussian curvature and topology of the structure. In the Appendix we describe the method of calculation of Minkowski functionals. Minkowski functionals are found to be a powerful tool to study evolution kinetics of block polymer morphologies.[33,45,46]

1. Kinetics of the gyroid-to-cylinder transition under an electric field. Fig. 10 shows Minkowski functionals for different electric field values. Crops of simulation snapshots are showed in the figure to highlight the kinetic pathway of the G-to-C transition. Each graph (V, S, $2H$ and χ) starts from the same value (the same for all electric fields), which corresponds to the initial gyroid structure from Fig. 2. First, we will describe the pathway for the strongest electric field (black solid lines). At the initial stage (10 time steps) the volume V and the surface S decrease, due to a partial melting of the structure under the applied electric field. Decreasing the volume in Fig. 10 does not contradict with the total mass conservation. The total volume of the block copolymer melt remains the same. The volume shown in the Fig. 10 is the volume occupied by one of block components inside a chosen iso-surface (for an extensive discussion of this issue see ref. 45). Partial melting of the structure can be also seen in a very slight increase in the curvature, $2H$. This is due to decrease of the local radii of curvature. The topology of the structure remains unchanged: the Euler characteristic χ remains the same. Its value is negative, which corresponds to a highly interconnected structure. A simulation snapshot (in the top left corner) confirms the conclusion, that the topology of the gyroid structure remains intact. The situation changes drastically at 30 time steps. Both the volume V and surface S reach the minimum values, reflecting a further melting of the structure. The Euler characteristic χ demonstrates an onset of the decrease, which means formation of new interconnections in the structure. These new interconnections appear as very thin cylinders (small radii), which should lead to an increase of the total mean curvature. Indeed, the curvature graph, $2H$, has a sharp peak at 30 time steps. The simulation snapshot (in the top left corner, second image) illustrates the formation of the first interconnections between gyroid tripods. These are the first five-fold connections. After that stage the volume V and the surface S start to recover reflecting growth of the structures in the electric field direction. At 3000 time steps the volume of the cylindrical phase will be almost the same regardless of the value of the applied electric field. At 60 time steps we observe a drastic drop in the Euler characteristic. This is due to the formation of many new connections through out the block polymer structure. These are five-fold connections shown in the simulation snapshot in Fig. 10, top right corner. The schematic cartoon in the figure (top right) illustrates how the five-fold connections grow from the gyroid tripods under an applied electric field. After about 80 time steps the Euler characteristic χ starts to increase: connections perpendicular to the electric field start to break (see also Fig. 4). The surface area S reaches the maximum at a slightly later stage, 100 time steps, as at this moment newly formed connections increase their thickness (see simulation snapshot in the lower left corner). This increase in thickness of new connections is one of the reasons that the mean curvature $2H$ reaches the minimum at the same time, 100 time steps. The second phenomenon

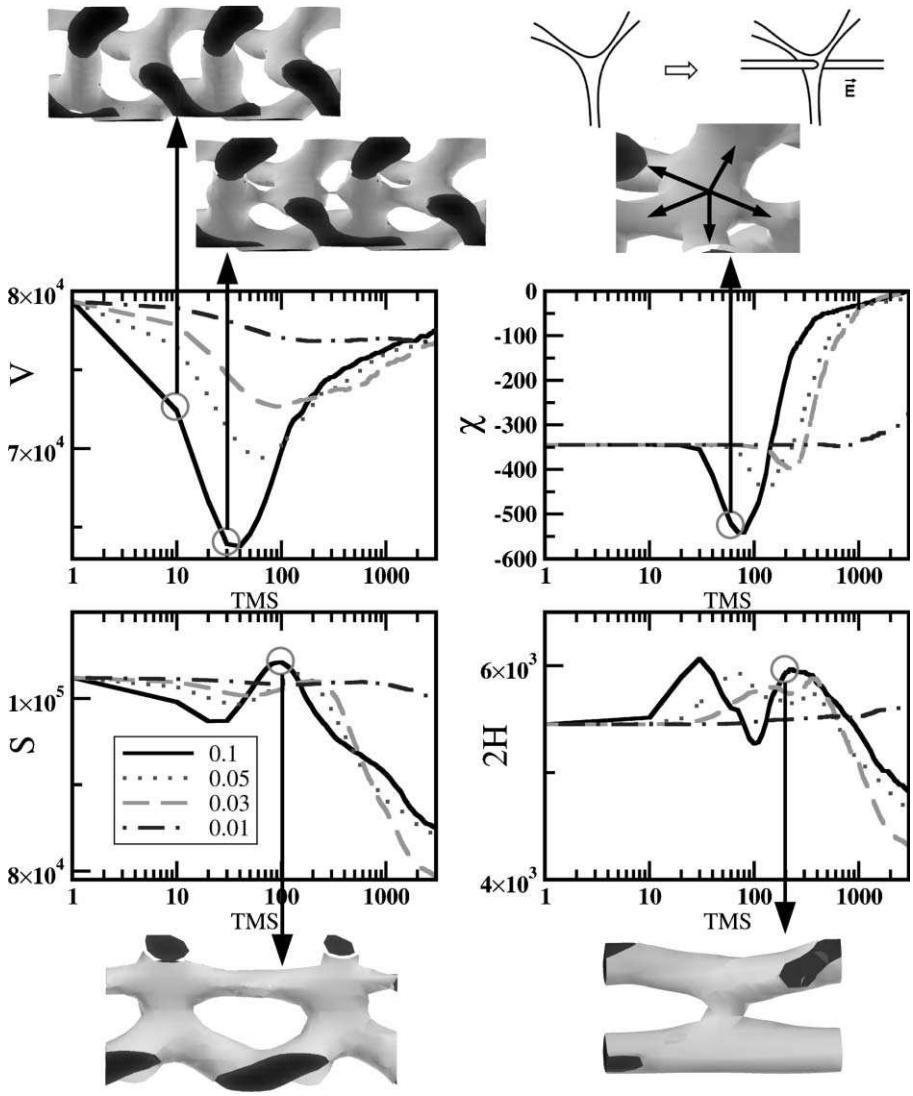

Fig. 10 Minkowski functionals as a function of time step (TMS) for different strengths of electric field $\tilde{\alpha}$ shown in the inset. A voxel is black if $\psi < -0.30$ (see also ref. 33). Examples of simulations are shown at the top and at the bottom.

which contributes to the drop of the mean curvature $2H$ is flattening of the five-fold connections (see the "man"-like structure in the snapshot in Fig. 10 and also Fig. 4b). Just before the connections, which are perpendicular to the electric field lines, break, they become thinner (simulation snapshot in the lower right corner of the Fig. 10). Because of that the mean curvature $2H$ increases reaching the second maximum at about 200 time steps. After the interconnections are broken, the cylinders become more and more straight which is reflected in the fall of both the surface area S and mean curvature $2H$. Both of these values are lower than the corresponding ones for the highly interconnected gyroid. At the end, the Euler characteristic becomes zero for every applied electric field, which corresponds to the case of the cylinders spanning the whole simulation box with no interconnections. Due to the periodic boundary condition each cylinder is topologically seen as a torus, contributing zero to the total Euler characteristics. The Minkowski functionals provide information about the final cylindrical structure as well. The volume V is the same for every electric field (3000 time steps). The surface area S and the mean curvature $2H$, for the system with $\tilde{\alpha} = 0.03$, are lower compared to the systems with $\tilde{\alpha}$= 0.1 and 0.05. This can be possible if the final cylinders for the system with $\tilde{\alpha} = 0.03$ have larger radii compared to the system with $\tilde{\alpha} = 0.1$. Indeed, the visual inspection of the real-space images shows that the number of cylinders for the system with $\tilde{\alpha} = 0.03$ is smaller compared to the system with $\tilde{\alpha} = 0.1$. This is attributed to the defects in the cylinders' packing. The Euler characteristic at 3000 time steps for both electric fields confirms the systems consists only of cylinders. The total volume V is the same but the cylinder radii for the system with $\tilde{\alpha} = 0.03$ are about 10% larger than for the system with $\tilde{\alpha}$.

General futures of all Minkowski functionals for different electric fields are similar. The important difference is that the Euler characteristic decreases much less for weaker electric fields. It means that the number of five-fold connections in the system is smaller compared to the case of a strong electric field. Therefore, another type of mechanism should occur in the gyroid-to-cylinder transition. This is illustrated in Fig. 11. The system with $\tilde{\alpha}$ forms five-fold connections but the number of these

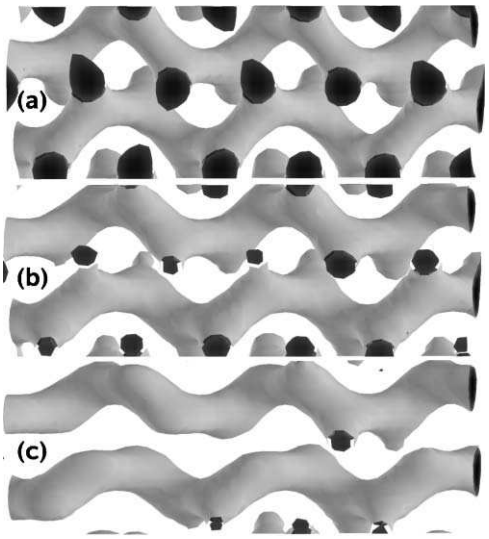

Fig. 11 Crops of simulation boxes for the gyroid structure under an electric field $\tilde{\alpha} = 0.03$. *Timesteps* : (*a*)100; (*b*)290; (*c*)500.

connections is smaller compared to systems under stronger electric fields. This is reflected in a much smaller drop in the Euler characteristic in Fig. 12. However, another mechanism becomes dominant. First, the gyroid structure becomes stretched under the electric field. Then, the gyroid connections, which are perpendicular to the electric field lines, break and the system transforms to helically wound cylinders (Fig. 11). As time proceeds, these cylinders straighten. During this process the cylinders adjust their position in space, and, therefore, this transition does not follow the same epitaxial pathway as for the system under strong electric fields from Fig. 4.

The Euler characteristic graph shows that after an electric field is applied, the gyroid structure survives for some time before the transition to cylinders occurs (initial plateau in Fig. 10, χ plots). We call this state an "excited gyroid". The situation of the "excited" structure is similar to the one observed in the reorientation of cylinders in an electric field (see ref. 37, Fig. 7).

We evaluate the life-time τ of an "excited" structure from the χ graphs in Fig. 10 as the time span from $t = 0$ (when the electric field is applied) till the moment when the Euler characteristic reaches the minimum. The result is shown in Fig. 13. The values of the life-time diverge as the strength of the electric field decreases. This suggests that we can discuss this transition in terms of critical phenomena. This can be understood as follows. The electrostatic contribution to the free energy renormalises the coefficient of the ψ^2 term in the free energy.[47] Such a change causes a critical phenomena. We fit the data using the argument of critical exponents, as is shown in Fig. 13. We can distinguish two regions. The first region exhibits one kinetic pathway illustrated in the Fig. 13, whilst in the second region there are two kinetic pathways: one is the same as in the region I and another is associated with the five-fold connections (the latter one being dominant mechanism). The two regions exhibit a somewhat different critical exponent, $p = 1.26$ (for region I) and $p = 1.5$ (for region II). The transition time diverges at non-zero value of electric field

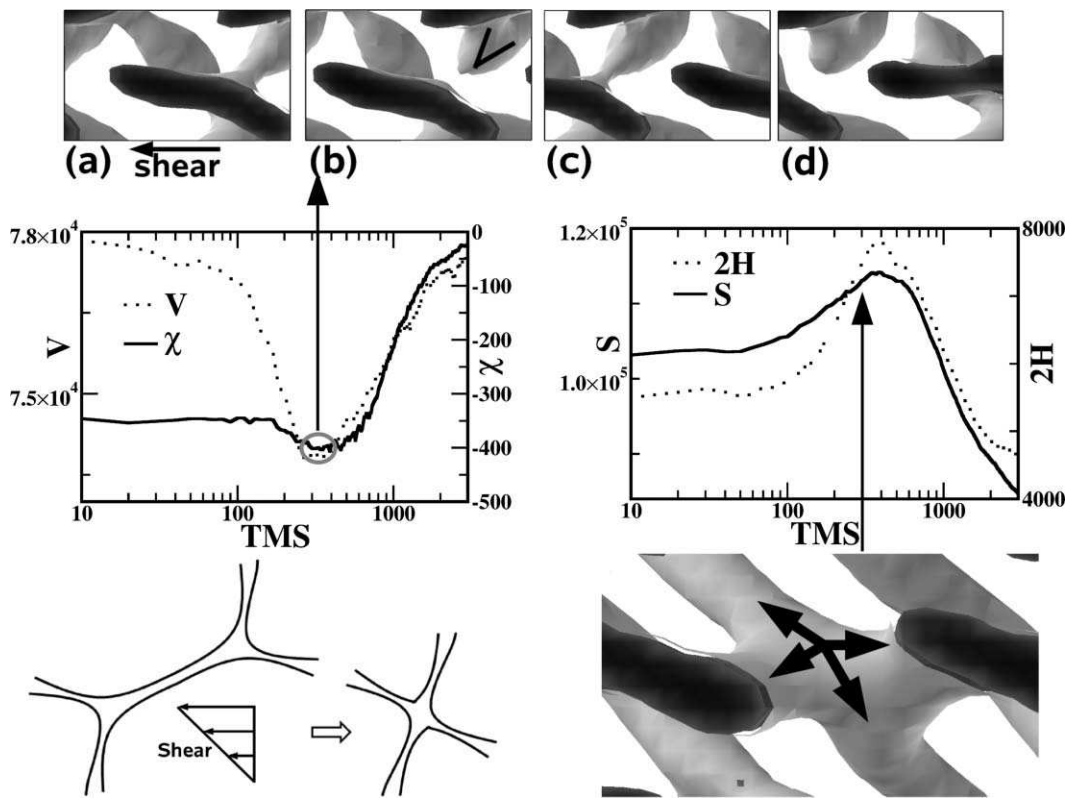

Fig. 12 Minkowski functionals as a function of time steps for the system in shear flow $\tilde{\dot{\gamma}} = 0.005$. Top: Crops of the simulation boxes for the system from Fig. 7. Time steps: (a) 290; (b) 300; (c) 310; (d) 320. "V" indicates a V-shape connection. Bottom: cartoon and snapshot illustrate the formation mechanism of a four-bond connection. A voxel is black if $\psi < -0.30$.

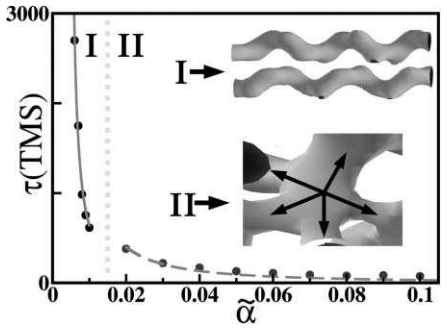

Fig. 13 Characteristic time for the gyroid-to-cylinder transition *versus* electric field strength. Circles: simulation results. Lines: best fitting by the function $\tau \approx (\tilde{\alpha}-\tilde{\alpha}_0)^P$. Inset: representative mechanisms in regions I and II.

as seen in Fig. 13. In the Landau theory of the phase transition of the second order, the correlation length behaves as $\xi \sim (T - T_c)^{-1/2}$ in the vicinity of the critical temperature T_c. As the electrostatic contribution to the free energy is proportional to $E_0^2\psi^2$ we have $(T-T_c) \sim (\tilde{\alpha}-\tilde{\alpha}_0)$. Therefore, $\xi \sim \tau^{1/3}$ (for p = 1.5) and $\xi \sim \tau^{0.4}$ (for p = 1.26). The exact nature of these critical exponents requires further theoretical investigation. However, we mention that in the Lifshitz–Slyozov theory the time evolution of the characteristic length of a conserved order parameter follows $\tau^{1/3}$,[47] the same power law as we observe in region II, Fig. 13.

For the electric fields $\tilde{\alpha} \geqslant 0.02$ both pathways coexist with five-fold connections being dominant for stronger fields and "curly cylinders" being dominant for weaker fields. For very weak electric fields, $\tilde{\alpha} \leqslant 0.01$, we do not observe any five-fold connections (only a couple of irregular connections form in the whole simulation box).

2. Kinetics of the gyroid-to-cylinder transition under shear flow. In this subsection we present results on Minkowski functionals analysis for the gyroid phase under shear flow, Fig. 12. The results are drastically different from the case of an electric field (Fig. 10). After the shear is applied the volume decreases which corresponds to a partial shear melting. The volume V reaches the minimum at about 300 time steps. Corresponding simulation snapshots in Fig. 9 (right) confirm that the gyroid network becomes thinner compared to the structure before the shear was applied (see also Fig. 9a right). At this stage the network connections break and reconnect in the direction of the flow (see also Fig. 9f, right). After all the cylinders are formed in the direction of the flow, the volume V recovers (Fig. 12). The Euler characteristic χ reaches the minimum at about the same time. Its minimum is very shallow compared to the case of the electric field, Fig. 10. This difference is due to the fact that we do not observe many connections forming in the sheared gyroid contrary to the five-fold connections in the case of the electric field. Fig. 9, right, shows only a few singular connections (snapshots d and e, right). The main mechanism for the gyroid-to-cylinder transition under shear is schematically illustrated in Fig. 12, bottom left (see also the discussion of Fig. 9 in the subsection III D). This pathway does not change the topology of the network and therefore does not contribute to the Euler characteristic. An example of a typical four-fold connection is shown in Fig. 12 (bottom right). Another difference between the Euler characteristic in the case of shear and in the case of the electric field is that the Euler characteristic in Fig. 12 is very "shaky" compared to the one in Fig. 10. This behaviour can be clarified by the simulation snapshots in Fig. 12 (top). One of the arms of what was the three-fold G-connection periodically breaks and reconnects while moving with the flow. As result, a typical V-shape "elbow" forms as an intermediate in this transition. A similar situation with propagation of the V-shape connection in the gyroid structure under shear was found in ref. 18. The volume V and the Euler characteristic χ reach their minima at approximately the same time. This can be explained by the fact that the formation of new connections (more negative Euler characteristic χ) happens when the system experiences the maximum stretching (maximum shear melting resulting in a drop in the volume V), see Fig. 9e, right.

The behaviour of the surface area S and the mean curvature $2H$ under shear flow are even more different (compared to V, χ graphs) from the corresponding behaviour under an electric field. In the case of the electric field, the surface area S and the mean curvature $2H$ have very different trends: when one has a maximum the other has a minimum and vice versa. In the case of shear flow both the surface area S and the mean curvature $2H$ have their only maxima at the same moment in time. Increase in the surface area S can be attributed to the structure stretching by shear. At the same time the bicontinuous network becomes thinner (Fig. 9e) which is reflected in the increase of the mean curvature $2H$. Formation of four-fold connections also contributes to the increase of the curvature $2H$. As it is illustrated by the cartoon in Fig. 12, the curvature radius between two arms in a four-fold connection is smaller compared to one between two arms in a three-fold connection.

IV. Conclusions

We performed a systematic investigation of the gyroid phase of a block copolymer melt under applied shear and electric fields using cell dynamics simulation. Kinetics of the gyroid-to-cylinder transition are found to be different under electric and shear flow. The values of the external fields and the resulting structures are shown in Table 1. The electric field should be above some non-zero threshold value to induce a transition to a cylindrical phase. Minkowski functionals are used to unravel various pathways of the transition in quantitative detail. Non trivial five- or four-fold intermediates are found. Our results complement similar studies by dynamic self-consistent field

Table 1 Summary of results for the gyroid subjected to different external fields

$\tilde{\alpha}$	Structure
0.001	Gyroid
0.01	Cylinders
0.1	Cylinders
$\tilde{\dot{\gamma}}$	
0.0001	Cylinders
0.0005	Cylinders
0.001	Cylinders
0.005	Cylinders

simulations,[18,24] and can serve as a study-precursor to investigate complex morphologies by a more time consuming SCF simulation. We found a second kinetic pathway of the transition under an electric field which was not observed in SCF simulation. These results can inspire real-space experimental study of the transition under electrical field.

After the paper was accepted we learnt about recent CDS study of the gyroid–lamellae interface.[48] We also note that very recently we developed a parallel CDS algorithm.[49]

Appendix: Minkowski functionals

To determine the details of the block copolymer phase transition kinetics we use Minkowski functionals that describe the morphological information contained in an image by numbers. Using these functionals we can describe very simple geometrical and topological quantities like the volume V, the surface area S, the mean curvature H, and the Euler characteristic χ.[45] The calculation is not a direct procedure; the first step is to generate a black and white image from the density fields and the second step is to study the behaviour of the four numbers as a function of time. The implementation used here is adapted from the work of Blasquez and Poiraudeau.[43] We briefly outline their algorithm (original publication in ref. 43 has a small misprint in their eqn 2). We describe the image by a set of cubic voxels [set to 1 (black) for the image and 0 (white) for the background]. It is possible to calculate four Minkowski functionals for the discrete 3D object in the following way: the volume ($V = n_3$), the surface area ($S = -6n_3 + 2n_2$), the mean curvature ($2H = 3n_3 - 2n_2 + n_1$), and the Euler characteristic ($\chi = -n_3 + n_2 - n_1 + n_0$) where n_3 is the number of open cubes, n_2 the number of open faces, n_1 the number of open edges and n_0 the number of open vertices. Following ref. 43 for each black voxel we examine only 13 neighbours called N_{ijk} where i, j, k indicate the position of the voxel in the box, and find the following contributions Δn_i for a black voxel N_{ijk}:

$$\Delta n_2 = 3 + Q(i, j, k-1) + Q(i, j-1, k) + Q(i-1, j, k) \quad \text{(A1)}$$

$$\Delta n_1 = 3 + Q(i, j, k-1)\, Q(i, j-1, k)\, Q(i, j-1, k-1) + Q(i, j, k-1)\, Q(i+1, j, k-1) + Q(i, j, k-1)\, Q(i, j+1, k-1) + Q(i, j, k-1)\, Q(i-1, j, k)\, Q(i-1, j, k-1) + Q(i, j-1, k)\, Q(i+1, j-1, k) + 2Q(i-1, j, k) + Q(i-1, j-1, k)\, Q(i, j-1, k)\, Q(i-1, j, k) + Q(i, j-1, k) \quad \text{(A2)}$$

$$\Delta n_0 = 1 + Q(i-1, j, k) + Q(i, j-1, k)\, Q(i+1, j-1, k) + Q(i-1, j-1, k)\, Q(i, j-1, k)\, Q(i-1, j, k) + Q(i, j, k-1)\, Q(i+1, j, k-1)\, Q(i+1, j-1, k)\, Q(i, j+1, k-1) + Q(i-1, j, k-1)\, Q(i, j, k-1)\, Q(i, j+1, k-1)\, Q(i-1, j+1, k-1)\, Q(i-1, j, k) + Q(i, j-1, k-1)\, Q(i+1, j-1, k-1)\, Q(i+1, j, k-1)\, Q(i, j, k-1)\, Q(i, j-1, k)\, Q(i+1, j-1, k) + Q(i-1, j-1, k-1)\, Q(i, j-1, k-1)\, Q(i, j, k-1)\, Q(i-1, j, k-1)\, Q(i-1, j-1, k)\, Q(i, j-1, k)\, Q(i-1, j, k) \quad \text{(A3)}$$

with $Q(i, j, k) = 1 - N_{ijk}$ where $N_{ijk} = 1$ for a black voxel (object) and $N_{ijk} = 0$ for a white voxel (background). The total numbers n_i are found by summation of Δn_i. The order of exploring the voxel grid is essential in determining the preceding neighbours: for eqn A1–A3 we first run index k, then j and finally i, while walking along the voxel grid.

Acknowledgements

This work is supported by Accelrys Ltd *via* an EPSRC CASE research studentship. All simulations were performed on the SGI Altix 3700 supercomputer at UCLan High Performance Computing Facilities. Communications with O. Mykhaylyk and T. Kawakatsu are gratefully appreciated. Table of contents image was made using a visualisation idea learnt from Frans van Hoesel.

References

1 I. W. Hamley, *The Physics of Block Copolymers*, Oxford University Press, Oxford, 1998.
2 *Nanostructured Soft Matter*, ed. A. V. Zvelindovsky, Springer, Dordrecht, 2007.
3 T. Hashimoto and K. Fukunaga, in *Nanostructured Soft Matter*, ed. A. V. Zvelindovsky, Springer, Dordrecht, 2007, ch. 2.
4 L. Tsarkova, in *Nanostructured Soft Matter*, ed. A. V. Zvelindovsky, Springer, Dordrecht, 2007, ch. 8.
5 T. Xu, J. Wang and T. P. Russel, in *Nanostructured Soft Matter*, ed. A. V. Zvelindovsky, Springer, Dordrecht, 2007, ch. 6.
6 A. Böker, in *Nanostructured Soft Matter*, ed. A. V. Zvelindovsky, Springer, Dordrecht, 2007, ch. 7.
7 I. W. Hamley, V. Castelletto and Z. Yang, in *Nanostructured Soft Matter*, ed. A. V. Zvelindovsky, Springer, Dordrecht, 2007, ch. 5.
8 I. Rychkov, *Macromol. Theory Simul.*, 2005, **14**, 207.
9 M. Schick, *Physica A*, 1998, **251**, 1.
10 K. Yamada, M. Nonomura and T. Ohta, *Macromolecules*, 2004, **37**, 5762.
11 A. C. Edrington, A. M. Urbas, P. DeRege, C. X. Chen, T. M. Swager, N. Hadjichristidis, M. Xenidou, L. J. Fetters, J. D. Joannopoulos, Y. Fink and E. L. Thomas, *Adv. Mater.*, 2001, **13**, 421.
12 T. Hashimoto, K. Tsutsumi and Y. Funaki, *Langmuir*, 1997, **13**, 6869.
13 D. Zhao, J. Feng, Q. Huo, N. Melosh, G. H. Fredrickson, B. F. Chmelka and G. D. Stuchy, *Science*, 1998, **279**, 548.
14 V. Z.-H. Chan, J. Hoffman, V. Y. Lee, H. Iatrou, A. Avgeropoulos, N. Hadjichristidis, R. D. Miller and E. L. Thomas, *Science*, 1999, **286**, 1716.
15 M. E. Vigild, K. Almdal, K. Mortensen, I. W. Hamley, J. P. A. Fairclough and J. Ryan, *Macromolecules*, 1998, **31**, 5702.
16 R. Eskimergen, K. Mortensen and M. E. Vigild, *Macromolecules*, 2005, **38**, 1286.
17 M. Imai, A. Saeki, T. Teramoto, A. Kawaguchi, K. Nakaya, T. Kato and K. Ito, *J. Chem. Phys.*, 2001, **115**, 10525.
18 T. Honda and T. Kawakatsu, *Macromolecules*, 2006, **39**, 2340.
19 M. Nonomura, K. Yamada and T. Ohta, *J. Phys.: Condens. Matter*, 2003, **15**, L423.
20 K. Yamada, M. Nonomura, A. Saeki and T. Ohta, *J. Phys.: Condens. Matter*, 2005, **17**, 4877.
21 G. Giupponi, J. Harting and P. V. Coveney, *Europhysics Lett.*, 2006, **73**, 533.
22 N. González-Segredo, J. Harting, G. Giupponi and P. V. Coveney, *Phys. Rev. E*, 2006, **73**, 031503.
23 M. W. Matsen, *Phys. Rev. Lett.*, 1998, **80**, 4470.
24 D. Q. Ly, T. Honda, T. Kawakatsu and A. V. Zvelindovsky, *Macromolecules*, 2007, **40**, 2928.
25 G. H. Fredrickson, *J. Rheol.*, 1994, **38**, 1045.
26 A. N. Morozov, A. V. Zvelindovsky and J. G. E. M. Fraaije, *Phys. Rev. E*, 2000, **61**, 4125.
27 M. Bahiana and Y. Oono, *Phys. Rev. A*, 1990, **41**, 6763.
28 T. Ohta, Y. Enomoto, J. L. Harden and M. Doi, *Macromolecules*, 1993, **26**, 4928.
29 H. Kodama and M. Doi, *Macromolecules*, 1996, **29**, 2652.
30 I. W. Hamley, *Macromol. Theory Simul.*, 2000, **9**, 363.

31 S. R. Ren and I. W. Hamley, *Macromolecules*, 2001, **34**, 116.
32 J. Feng and E. Ruckenstein, *J. Chem. Phys.*, 2004, **121**, 1609.
33 M. Pinna, A. V. Zvelindovsky, S. Todd and G. Goldbeck-Wood, *J. Chem. Phys.*, 2006, **125**, 154905.
34 T. Ohta, H. Nozaki and M. Doi, *J. Chem. Phys.*, 1990, **93**, 2664.
35 T. Taneike and Y. Shiwa, *J. Phys.: Condens. Matter*, 1997, **9**, L147.
36 A. V. Zvelindovsky and G. J. A. Sevink, *Phys. Rev. Lett.*, 2003, **90**, 049601.
37 K. S. Lyakhova, A. V. Zvelindovsky and G. J. A. Sevink, *Macromolecules*, 2006, **39**, 3024.
38 We note that eqn (12) in ref. 32 is valid only for symmetric lamellae, $f = 0.5$, as it was originally derived for the symmetric lamellae in our work.[40] The same comment is valid for eqn (11) in ref. 41 which is not correct for a cylindrical system. It should be also noted, that v is neither the volume of a monomer nor the volume of a bead, as we stated in some of our earlier papers (see discussion in ref. 37). It seems this little confusion crept into other literature.[41].
39 A. Knoll, K. S. Lyakhova, A. Horvat, G. Kraush, G. J. A. Sevink, A. V. Zvelindovsky and R. Magerle, *Nat. Mater.*, 2004, **3**, 886.
40 A. V. Kyrylyuk, A. V. Zvelindovsky, G. J. A. Sevink and J. G. E. M. Fraaije, *Macromolecules*, 2002, **35**, 1473.
41 X. Li, Y. Jiang, Y. Li and H. Liang, *ChemPhysChem*, 2006, **7**, 1693.
42 K. R. Mecke, in *The Art of Analysing and Modelling Spatial Structures and Pattern Formation. Lecture Notes in Physics*, ed. K. R. Mecke and D. Stoyan, Springer, Berlin, 2000, **Vol. 554**, p. 111.
43 I. Blasquez and J.-F. Poiraudeau, *J. WSCG*, 2003, **11**(1), ISSN 1213-6972.
44 K. Michielsen, H. De Raedt and J. T. M. De Hosson, *Advances in Imaging and Electron Physics*, 2002, **125**, 119.
45 G. J. A. Sevink and A. V. Zvelindovsky, *J. Chem. Phys.*, 2004, **121**, 3864.
46 G. J. A. Sevink, in *Nanostructured Soft Matter*, ed. A. V. Zvelindovsky, Springer, Dordrecht, 2007, ch. 9.
47 A. Onuki, *Phase Transition Dynamics*, Cambridge University Press, Cambridge, 2002.
48 K. Yamada and T. Ohta, *J. Phys. Soc. Jpn.*, 2007, **76**, 084801.
49 X. Guo, M. Pinna and A. V. Zvelindovsky, *Macromol. Theory Simul.*, 2007, **16**, DOI: 10.1002/mats.200700038.